Published in final edited form as:
ACS Nano. 2011 January 25; 5(1): 565–573. doi:10.1021/nn102697r.

Orienting Periodic Organic-Inorganic Nanoscale Domains Through One-Step Electrodeposition

David J. Herman[1], **Joshua E. Goldberger**[2], **Stephen Chao**[1], **Daniel T. Martin**[1], and **Samuel I Stupp**[*,1,2,3,4]

[1] Department of Materials Science and Engineering, Northwestern University, Evanston, Illinois 60208, USA

[2] Department of Chemistry, Northwestern University, Evanston, Illinois 60208, USA

[3] Department of Medicine, Northwestern University, Chicago, Illinois 60611, USA

[4] Institute for BioNanotechnology in Medicine, Northwestern University, Chicago, Illinois 60611

Abstract

One of the challenges in the synthesis of hybrid materials with nanoscale structure is to precisely control morphology across length scales. Using a one-step electrodeposition process on indium tin oxide (ITO) substrates followed by annealing, we report here the preparation of materials with preferentially oriented lamellar domains of electron donor surfactants and the semiconductor ZnO. We found that either increasing the concentration of surfactant or the water to dimethyl sulfoxide ratio of solutions used resulted in the suppression of bloom-like morphologies and enhanced the density of periodic domains on ITO substrates. Furthermore, by modifying the surface of the ITO substrate with the conductive polymer blend poly(3,4-ethylenedioxythiophene):poly(styrenesulfonate), we were able to alter the orientation of these electrodeposited lamellar domains to be perpendicular to the substrate. The long-range orientation achieved was characterized by 2D grazing incidence small angle X-ray scattering. This high degree of orientation in electronically active hybrids with alternating nanoscale p-type and n-type domains is of potential interest in photovoltaics or thermoelectric materials.

Keywords

electrodeposition; lamellar; Zinc Oxide; Zinc Hydroxide; hybrid; nanoscale; orientation; alignment

The controlled synthesis of electronically active organic-inorganic hybrid materials over multiple length scales is of great interest in optoelectronic applications.[1–3] One example is the useful hybrid photovoltaic morphology with an alternating nanoscale periodicity of 5–10 nm donor and acceptor domains for maximum exciton splitting.[4] However, in order for this nanoscale ordering to be the ideal one for devices it has to have a precise macroscopic orientation throughout the active device area in order to support efficient charge transport to the corresponding electrodes. Several methods exist to fabricate hybrid materials with controlled structural features at multiple length scales. In one approach, self-assembling organic molecules have been widely utilized to template the mineralization of various

[*] s-stupp@northwestern.edu.

Supporting Information Available: Supporting information includes SEMS of films electrodeposited at other growth conditions, water contact angle measurements, and 2D-GISAXS images with their corresponding 1D-functions of intensity *vs.* azimuthal angle φ. This material is available free of charge *via* the Internet at http://pubs.acs.org.

inorganic materials, such as SiO_2,[5] CdS,[6, 7] and a variety of other chalcogenides.[8] Although nanoscale assembly and periodicity of organic and inorganic domains can be controlled, orienting them macroscopically and uniformly on substrates *via* facile cost-effective approaches remains challenging. Other methods employ a combination of top down and bottom up strategies. These include the functionalization of solution grown nanowire arrays with organic molecules,[9–12] the infiltration of organic semiconductors into mesoporous inorganic films,[13] or the use of PDMS patterning to direct molecular self-assembly and mineralization.[14, 15] These multi-step techniques have potential scale up limitations.

Electrodeposition has recently gained much interest because it provides a one-step facile technique for synthesizing hybrid materials and it allows direct deposition of electronic materials onto electrodes such as indium tin oxide (ITO). A variety of electronically active inorganic materials have been electrodeposited, including ZnO,[16–19] SnO_2,[20] MnO_2,[21] $Co(OH)_2$,[22] and $Ni(OH)_2$.[23] For photoconductor[24] and photovoltaic devices,[11, 25, 26] ZnO is a material of particular interest because it is an n-type semiconductor with high electron mobility and often forms interfaces with organic semiconductors that are energetically favorable for exciton splitting.[27] Choi and co-workers demonstrated the deposition of lamellar Zn-rich inorganic domains and dodecyl sulfate domains with periodicities on the order of 2–3 nm.[18] Recently, we reported the incorporation of semiconducting surfactants into the electrodeposition bath, and successfully produced nanoscale lamellar $Zn(OH)_2$ with either pyrene or oligothiophene moieties on ITO.[3] Upon annealing, the inorganic phase was converted to ZnO, and the nanoscale ordering of p-type surfactant with n-type ZnO resulted in high performance photoconductors comparable to amorphous silicon. The conjugated nature of the surfactant leading to π-stacked assemblies was found to be critical in order to stabilize the lamellar architecture with nanoscale domains as $Zn(OH)_2$ converted into ZnO upon annealing.

One challenge that still remains in the electrodeposition of the photoconductive lamellar structures is how to control the macroscopic orientation of the lamellar domains on ITO surfaces. For optoelectronic devices, orienting these lamellar structures with their normal parallel to substrate surfaces will reduce the distance that photoexcited holes and electrons would have to travel before reaching the electrode. It has been previously reported that the orientation of the lamellar structures in the bulk can vary greatly with the nature of the surfactant used.[18, 28, 29] Most of these studies have shown either lamellar structures grown completely parallel to the substrate surface[29] or a distribution of stacking orientations with a majority of the lamellae still parallel to the substrate surface.[18] Here we report the preparation of hybrids using electrodeposition with lamellar domains of the semiconductor ZnO and the conjugated surfactant 1-pyrenebutyric acid (PyBA) as a model system. Using 2D grazing incidence small angle X-ray scattering (2D-GISAXS), we investigate the chemistry of the electrodeposition process to probe its role in the growth of oriented nanoscale lamellae over macroscopic scales.

RESULTS AND DISCUSSION

Hybrid materials with lamellar domains were electrodeposited in a solution of $Zn(NO_3)_2$•6 H_2O and PyBA surfactant using the cathodic reduction of nitrate in a mixed solvent bath of water/dimethyl sulfoxide (DMSO). This reaction increases the local pH near the working electrode surface resulting in the deposition of $Zn(OH)_2$,

$$NO_3^- + H_2O + 2e^- \rightarrow NO_2^- + 2\,OH^- \quad (E = 0.01\,V\ vs.\,NHE), \tag{1}$$

$$Zn^{+2} + 2\,OH^- \rightarrow Zn(OH)_2\,(s)\downarrow \quad (2)$$

DMSO was used as a co-solvent since it is miscible with water and helps solubilize the surfactant. ITO was used as the working electrode because of its importance in devices for optoelectronic functions. As demonstrated in our previous work,[3] the $Zn(OH)_2$ converts to ZnO upon annealing, and the lamellar structure of the film is maintained.

Figure 1 shows the results of electrodeposition at −0.9V at two different concentrations of PyBA in solution. At a surfactant concentration of 0.05 wt %, SEM images show that the dominant micron scale structure of the electrodeposited film is a bloom-like morphology, which we define as clusters of growth extending radially outwards from a center point of nucleation. In contrast, when the concentration of the PyBA is increased to 0.25 wt % we observe two-dimensional flake-like growths covering the substrate surface with a variety of orientations rather than the clusters of nucleation associated with the bloom morphology (Figure 1C). X-ray diffraction measurements of both films confirm the lamellar nanoscale periodicity, as evidenced by the integer ratio of peak positions extending to four orders or higher (Figure 1B, D). For the case of 0.05 wt % PyBA surfactant, the x-ray data in Figure 1B shows that the lamellar structure has a periodicity of 3.2 nm. For the case of higher surfactant concentration, a second smaller d-spacing emerges with a periodicity of 2.6 nm. This 0.6 nm change in spacing could be due either to the interdigitation of pyrene rings at high surfactant loadings, or a reduction in the thickness of the inorganic layer, but this was difficult to determine *via* TEM because of the minimal contribution of this spacing within the film, as evidenced by the weakly reflecting (00*l*)* peaks. For further visualization of the lamellar structure, a bright-field TEM image, taken from the sample showing bloom-like morphologies, is shown in Figure 1E. In this TEM image, the electron-rich inorganic phase appears darker and the less electron-rich PyBA organic domain appears lighter. Figure 1 demonstrates our ability to dictate hybrid micron scale morphology simply by changing the surfactant concentration in solution.

To further investigate the effects of surfactant concentration on the nucleation and growth of structures, we electrodeposited films for a very short time and analyzed their growth *via* SEM. As observed in Figure 2A, sparse nucleation on the substrate surface occurs for films electrodeposited for 1 minute in a solution with 0.05 wt % of PyBA. Furthermore, the onset of bloom-like structure is readily observed. In this case, the bloom-like growth appears to originate from a flat footprint region that nucleates first. We believe that at low surfactant concentrations, surface assemblies of surfactant molecules are too sparse to nucleate a dense number of structures. In addition, since the voltage is kept constant throughout the electrodeposition process, it is well known that a depletion region can develop within a short distance from the electrode surface after only a short time.[30] When this occurs, growth of pre-nucleated structures is favored over the nucleation of new sites on the electrode. This occurs as precursors diffuse from the bulk towards the electrode surface and contribute to the growth of pre-existing structures before reaching the inner-most nucleation plane. Thus, at the surface of the electrode itself, a short time into the deposition, the local surfactant concentration is too low near the electrode surface to form a dense number of nuclei. We believe that this type of concentration-limited nucleation, followed by fast growth, results in the bloom-like morphology observed for the case of 0.05 wt% PyBA.

For the case of higher surfactant concentration, a greater amount of surfactant is present near the substrate surface throughout the deposition, allowing for more nucleation to occur. In Figure 2B, an SEM image of a substrate electrodeposited for 1 minute in the solution with 0.25 wt % PyBA is shown, suggesting greater nucleation under these conditions.

Furthermore, instead of a footprint and bloom-like morphology, this substrate shows a distribution of parallel structures and perpendicular structures growing directly on the substrate surface. Thus, the increase in surfactant concentration allows for the direct nucleation and growth of flake-like structures from the substrate surface instead of bloom-like clustering. Finally, although the films formed at higher concentration lack bloom-like growths, the flake-like structures containing the alternating inorganic and organic domains still look orientationally isotropic when viewed by top-down SEM (Figure 1C).

Given the strong effect of surfactant concentration on structure, we hypothesized that varying the solvent composition of the solution might also affect the aggregation of surfactant molecules and therefore film morphology. PyBA molecules are more soluble in solutions with a greater volume fraction of DMSO, and should therefore be less aggregated than in solutions with higher fractions of water. Figure 3 shows the results for varying the solvent composition in solution when the concentration of surfactant is equal to 0.05 wt %. At a solution composition of 35:65 (*v/v*) H_2O/DMSO, the film nucleates sparsely on the substrate surface, as seen in Figure 3A, and the structures that are present grow with the bloom-like morphology described previously. As the proportion of water in the solution is increased to 50% and then to 65%, the morphology transitions from a bloom-like structure (Figure 1A and 3B) to a flake-like morphology, as revealed by Figure 3C. Interestingly, in contrast to the unoriented flake-like structures grown at high surfactant concentrations and 50% H_2O (Figure 1C), the flake-like structures grown at low surfactant concentration and 65% H_2O appear aligned and oriented vertically to the substrate surface. Finally, the TEM image in Figure 3D shows that the nanoscale lamellar assembly of inorganic and organic domains is still maintained under these conditions of electrodeposition.

In an effort to understand why hybrid films grown from solutions with higher water content consist of vertically oriented flake-like structures, we studied the early nucleation and growth of these films. Figure 3E shows an SEM image for an ITO substrate electrodeposited for 30 seconds. Even after short deposition times, the substrate shows many regions of dense nucleation, as well as regions of more sparse growth. This is in sharp contrast to the case when only 50% water is in the solution, which shows only sparse nucleation and bloom-like growth, as was already described in Figure 2A. Thus, increasing the water ratio in solution results in a dramatic change of macroscale morphology, while maintaining the nanoscale lamellar domains. With increasing water content in the solvent, we expect more PyBA micelles both in the solution and on the substrate surface as a result of increased hydrophobic interactions among pyrene moieties. Micelles should be highly effective nucleating agents as they deposit many contiguous molecules at once on the substrate, placing more surfactant at the inner nucleation plane for dense nucleation and oriented growth. Finally, the increase in water makes the electrochemical reaction more favorable, as shown in equation (1), which may also lead to a greater amount of nucleation. From the results presented thus far, it appears that by targeting surfactant aggregation, either by increasing the surfactant concentration or increasing the water composition in solution, denser nucleation can occur on the substrate surface, resulting in individual flake-like growth instead of bloom-like clustering. We also explored the effect of changing $Zn(NO_3)_2$ concentration and of adding KCl as a supporting electrolyte to the solution, but these parameters did not show pronounced changes to bloom-like morphologies when added to a solution of 0.05 wt % PyBA and 50:50 (v/v) H_2O/DMSO (Supplemental).

To quantify the degree and type of nanoscale lamellar orientation extending throughout the bulk of the films, 2D grazing incidence small angle X-ray scattering (2D-GISAXS) was used. 2D-GISAXS is a non-destructive x-ray scattering technique that is surface sensitive and has been used to characterize nanoparticles and nanostructures on surfaces.[31–33] In this technique, a well-collimated x-ray beam is directed at the substrate surface with an

incidence angle close to the critical angle of the substrate. Because the incidence angle is very small, the x-ray beam samples a large area of the substrate, resulting in an increase in scattering signal as compared to other x-ray techniques. In addition, because the scattering signal is recorded with a 2D detector, both in-plane and out-of-plane structure can be analyzed.

Figure 4 shows 2D-GISAXS data for the film grown in 50% water and exhibiting bloom-like morphologies (Figure 1A, Figure 3B) and for the film grown in 65% water, which exhibits vertically oriented flakes (Figure 3C). In each case, the 2D-GISAXS data shows at least five rings of scattering, indicating the high degree of ordering within the lamellar domains. For the bloom-like morphology, the 2D-GISAXS in Figure 4A shows the strongest scattering intensity in the vertical direction ($\varphi = 90^{\circ}$), characteristic of lamellar structures with the majority of stacking parallel to the substrate surface ($\alpha_{lamellar} = 0^{\circ}$), as shown in Figure 5A. A plot of the (001) ring intensity as a function of azimuthal angle, φ shows that for the bloom-like morphology, 71.4% of the scattering intensity is between $45^{\circ} \leq \varphi \leq 90^{\circ}$, with 44.3% of the overall scattering intensity between $67.5^{\circ} \leq \varphi \leq 90^{\circ}$ (see supplemental). Thus, the predominant orientation of the lamellar structures is parallel to the substrate surface.

We also quantified the orientation of the lamellar structures for the film grown with 65% water and exhibiting single flake-like growths. From the SEM shown in Figure 3C, one might expect the 2D-GISAXS data to show predominantly perpendicular orientation of the lamellar domains, as shown schematically in Figure 5B. Surprisingly, the majority of the lamellar stacking orientation is still more parallel than perpendicular to the substrate surface (Figure 4B). Plotting the (001) ring intensity as a function of φ and applying the appropriate integration limits reveals that 57.9% of the scattering intensity is between $45^{\circ} \leq \varphi \leq 90^{\circ}$. This is a 13.5% decrease when compared to the bloom-like morphology, but the SEM image of Figure 3C might lead one to expect an even greater decrease.

Referring back to the early nucleation and growth SEM images in Figure 2A and Figure 3E, we hypothesize that the UV-ozone treated ITO preferentially nucleates and grows lamellar structures with parallel orientation first, irrespective of the chemistry of the electrodeposition solution. After the initial parallel nucleation, lamellar structures with off-parallel orientations can nucleate and grow on top of the initially deposited parallel lamellar surface. We confirmed this growth mechanism by using 2D-GISAXS to study the early nucleation and growth for the case of electrodeposition in a solution of 0.05 wt % PyBA and 50:50 (*v/v*) H_2O/DMSO. Figure 6 shows the 2D-GISAXS data for films electrodeposited for 30 seconds and for 1 minute. Figure 6A clearly shows scattering intensity only for parallel orientation of the lamellar domains after 30 seconds of electrodeposition. Scattering associated with perpendicular orientation only occurs at the later time point, as seen in Figure 6B. From these data, it is apparent that the parallel orientation of the lamellar domains nucleates first, followed by off-parallel orientation. Thus, even though changes in the aggregation of surfactant molecules as mediated by solution chemistry can result in different morphologies, the substrate surface also has a large effect on the initial nucleation and growth processes.

Because it is known that different substrates can induce large changes in the type of surfactant aggregation occurring on a surface,[34] we decided to coat the ITO surface with poly(3,4-ethylenedioxythiophene):poly(styrenesulfonate) (PEDOT:PSS). PEDOT:PSS is a material that is commonly used to modify ITO substrates in optoelectronic devices, in order to decrease the substrate surface roughness and also to function as an electron blocking layer in solar cells.[35, 36] In addition, the PEDOT:PSS changes the surface energy of the substrate,

making it more hydrophobic than UV-ozone treated ITO, as we confirmed through water contact angle measurements (Supplemental).

Figure 7 shows the results of electrodeposition at −0.9V on PEDOT:PSS coated ITO with the dilute 0.05 wt % concentration of PyBA. Without surface modification, this solution chemistry resulted in bloom-like growth (Figure 1A), but with PEDOT:PSS, the morphology is now flake-like, as seen in Figure 7A. The multiple rings in the 2D-GISAXS pattern in Figure 7B and the TEM image in Figure 7C confirm that the nanoscale lamellar structure is still present. 2D-GISAXS characterization (Figure 7B) further reveals that the lamellar domains possess a high degree of perpendicular alignment with respect to the substrate film. Plotting the (001) ring intensity as a function of φ and applying the appropriate integration limits reveals that 84.6% percent of the scattering intensity is between $0^{\circ} \leq \varphi \leq 45^{\circ}$. Thus, interestingly, the predominant orientation of the inorganic-organic lamellar domains on PEDOT:PSS surfaces is perpendicular instead of parallel to the substrate.

This perpendicular growth on PEDOT:PSS coated electrodes occurs even at short electrodeposition times. Figure 7D shows an SEM image for a PEDOT:PSS coated ITO substrate that underwent electrodeposition for 1 minute. As can be seen in this figure, the 2D flake structures grow individually and extend vertically upwards directly from the substrate surface. This is in direct contrast to the early nucleation and growth seen for the same solution chemistry on the UV-ozone treated ITO surface (Figure 2A). In both cases, sparse nucleation occurs on the substrate surface, but in the case when PEDOT:PSS is used, flakes grow directly upwards from the substrate surface, ultimately resulting in high density films with alternating inorganic and organic domains.

It is clear that the surface structure of the PEDOT:PSS layer on the substrate plays a critical role in determining the larger scale morphology of electrodeposited lamellar nanoscale domains. We speculate that the amphiphilic nature of the coated substrate with both hydrophobic thiophene moieties and hydrophilic sulfonic acid and ethylene oxide groups increases both the affinity of pyrene functions and Zn^{+2} ions to the surface. This way, the hydrophobic patches of PEDOT:PSS would allow assemblies of surfactant molecules to form which in turn promote perpendicular growth. In terms of the inorganic phase, since single $Zn(OH)_2$ is known to grow as two-dimensional sheets with an excess of positive charge on the 2-D face,[37, 38] small surface patches of both charged and hydrophobic character may favor nucleation of lamellar domains with perpendicular orientation. It follows that on a hydrophilic substrate, the charged face of the 2-D $Zn(OH)_2$ crystal promotes growth of lamellae parallel to the substrate. In this case, the lamellar phase can then proceed to grow in a step-by-step fashion, whereby the organic molecule assembles on the surface of the $Zn(OH)_2$ and subsequently nucleates the next layer of inorganic. This process then repeats, creating the parallel lamellar structure, as has been argued in other work.[29]

In order to support the hypothesis proposed above, we electrodeposited hybrid material on ITO substrates coated with a 0.1 wt.% solution of poly(styrenesulfonate) (PSS). We found that the hydrophilic PSS layer indeed causes the dense nucleation and growth of lamellar domains that are predominantly parallel to the substrate (see Figure 7E and 7F). Thus, we propose that in the case of PEDOT:PSS, the hydrophobicity of the substrate surface favors the aggregation of pyrene moieties on the hydrophobic regions, whereas the hydrophilic regions should favor the accumulation of Zn^{+2} ions, together resulting in the growth of perpendicular alternating domains.

Conclusions

The orientation and density of alternating inorganic and organic nanoscale domains using electrodeposition can be effectively controlled through solution and substrate chemistry. In the case of zinc hydroxide (a precursor to the semiconductor ZnO) and amphiphilic molecules, parallel orientation of the lamellar structure is easily attained on hydrophilic surfaces. However, perpendicular orientation of the 2D lamellar domains is possible in the presence of an inhomogeneous surface with both hydrophobic and hydrophilic regions. This type of orientation of nanoscale lamellar hybrids with optoelectronic properties is of great interest for photovoltaics where the nanoscale favors exciton splitting and the perpendicular orientation at longer length scales favors efficient charge transport to electrodes.

Experimental Methods

Solutions were composed of varying concentrations of $Zn(NO_3)_2 \bullet 6H_2O$ (Aldrich, 98%) and 1-pyrenebutyric acid (PyBA, Aldrich, 97%) in a mixture of dimethylsulfoxide (DMSO) and H_2O. The solutions were stirred and purged with Ar gas at 80 °C for 20 min prior to deposition. All solutions were adjusted to a pH of 5.35 by adding 0.1 M NaOH drop wise to the solution.

Indium tin oxide (ITO) coated glass (10 Ω/sq sheet resistance, Kintec) was first scrubbed with soap water, and then cleaned under sonication with subsequent baths of water, acetone, methanol, and water, respectively, and finally dried with N_2 gas. For depositions on bare ITO, the substrate was UV-ozone treated for 10 min prior to electrodeposition, and placed upright in the cell, functioning as the working electrode. For ITO coated with polymer (either PEDOT:PSS (Clevios™ P VP AI 4083, H.C. Starck) or PSS (0.1 wt % in water, 1 MDa avg MW)), the ITO was first UV-ozone treated for 30 minutes followed by an immediate layer of polymer spin-cast on top of the substrate with a 15 s ramp from 0 rpm to 4,000 rpm for a total spin time of 1 minute. The polymer coated substrates were then baked on a hot plate at 120 °C for 20 minutes. The thickness of the polymer layer was approximately 45 nm.

Electrodepositions were performed using an EG&G Princeton Applied Research Potentiostat (model 263A) in an undivided cell vial using a three-electrode set-up and 6 mL of the solution described above. Zn wire (Alfa Aesar, 99.9997%) was used as a counter electrode and a Ag/AgCl electrode (BAS Inc. model RE-5B) was used as the reference. The working electrode was either UV-ozone treated ITO, or PEDOT:PSS coated ITO. For all depositions, the applied potential was −0.9 V, the temperature was maintained at 80 °C, and the solutions were under constant magnetic stirring. After deposition, films were rinsed with water and dried with N_2 gas.

Morphologies were characterized using a Hitachi S-4800-II FE SEM operating at 3 kV. The lamellar nanostructure was investigated with a JEOL JEM-2100F FAST TEM operating at 200 kV. X-Ray reflectivity measurements were recorded on a Rigaku ATX-G Thin-film Diffractometer utilizing Cu Kα radiation. 2D-GISAXS measurements were obtained using a Rigaku MicroMax-002+ High-Intensity Microfocus Sealed Tube X-ray Generator (Cu Kα radiation) with either a Bruker Hi-Star 2-D wire detector or Fujifilm phosphor image plate. 2D-GISAXS data for the early nucleation and growth was obtained at beamline 12-ID-C at the Advanced Photon Source, Argonne National Laboratory. All 2D-GISAXS measurements were performed at an angle close to the critical angle of the ITO.

To quantify the amount of scattering corresponding to various orientations, the ring of scattering associated with the (001) lamellar peak was unwrapped into a 1-D function of intensity, I(φ), versus azimuthal angle, φ. To determine the percent of scattering associated

with lamellar structures oriented between the angles $\varphi_{initial}$ and φ_{final}, the 1D scattering data was integrated between these bounds and divided by the total scattering intensity, according to the equation:

$$\frac{\int_{\varphi_{initial}}^{\varphi_{final}} I(\varphi)\, d\varphi}{\int_{0^\circ}^{90^\circ} I(\varphi)\, d\varphi}$$

Finally, because the scattering intensity I(φ) is symmetric around φ = 90º, we limited our interest to the region 0º≤ φ ≤ 90º.

Supplementary Material

Refer to Web version on PubMed Central for supplementary material.

Acknowledgments

This work was supported mostly by DOE grant DE-FG02-00ER54810 from Basic Energy Sciences and partial support from the Non-Equilibrium Energy Research Center (NERC), an Energy Frontier Research Center funded by the U.S. Department of Energy, Office of Science, Office of Basic Energy Sciences under Award Number DE-SC0000989. DJH is supported by a DoD, Air Force Office of Scientific Research, National Defense Science and Engineering Graduate (NDSEG) Fellowship, 32 CFR 168a, and JEG was supported by Award Number F32EB007131 from the National Institute of Biomedical Imaging and Bioengineering. The content is solely the responsibility of the authors and does not necessarily represent the official views of the National Institute Of Biomedical Imaging And Bioengineering or the National Institutes of Health.

The SEM and TEM work was performed at the Electron Probe Instrumentation Center (EPIC) of Northwestern University Atomic- and Nanoscale Characterization Experimental Center (NUANCE). NUANCE Center is supported by NSF-NSEC, NSF-MRSEC, Keck Foundation, the State of Illinois, and Northwestern University. X-ray measurements were performed at J. B. Cohen X-ray Facility supported by the MRSEC program of the National Science Foundation (DMR-0520513) at the Materials Research Center of Northwestern University. Use of the Advanced Photon Source at Argonne National Laboratory was supported by the U. S. Department of Energy, Office of Science, Office of Basic Energy Sciences, under Contract No. DE-AC02-06CH11357.

References

1. Rolison DR, Long JW, Lytle J, Fischer AE, Rhodes CP, McEvoy TM, Bourg ME, Lubers AM. Multifunctional 3D Nanoarchitectures for Energy Storage and Conversion. Chem Soc Rev. 2009; 38:226–252. [PubMed: 19088976]
2. Sanchez C, Boissiere C, Grosso D, Laberty C, Nicole L. Design, Synthesis, and Properties of Inorganic and Hybrid Thin Films Having Periodically Organized Nanoporosity. Chem Mater. 2008; 20:682–737.
3. Sofos M, Goldberger J, Stone DA, Allen JE, Ma Q, Herman DJ, Tsai WW, Lauhon LJ, Stupp SI. A Synergistic Assembly of Nanoscale Lamellar Photoconductor Hybrids. Nature Materials. 2009; 8:68–75.
4. Coakley KM, Liu Y, Goh C, McGehee MD. Ordered Organic-Inorganic Bulk Heterojunction Photovoltaic Cells. MRS Bulletin. 2005; 30:37–40.
5. Sofos M, Stone DA, Goswani DK, Okasinski JS, Jin H, Bedzyk MJ, Stupp SI. Nanoscale Structure of Self-Assembling Hybrid Materials of Inorganic and Electronically Active Organic Phases. J Phys Chem C. 2008; 112:2881–2887.
6. Braun PV, Osenar P, Stupp SI. Semiconducting Superlattices Templated By Molecular Assemblies. Nature. 1996; 380:325–328.
7. Osenar P, Braun PV, Stupp SI. Lamellar Semiconductor-Organic Nanostructures From Self-Assembled Templates. Adv Mater. 1996; 8:1022–1025.

8. Huang X, Li J. From Single to Multiple Atomic Layers: A Unique Approach to the Systematic Tuning of Structure and Properties of Inorganic-organic Hybrid Nanostructured Semiconductors. J Am Chem Soc. 2007; 129:3157–3162. [PubMed: 17319658]
9. Briseno AL, Holcombe TW, Akram BI, Garnett EC, Shelton SW, Frechet JJM, Yang P. Oligo- and Polythiophene/ZnO Hybrid Nanowire Solar Cells. Nano Letters. 2010; 10:334–340. [PubMed: 20000808]
10. Martini C, Poize G, Ferry D, Kanehira D, Yoshimoto N, Ackermann J, Fages F. Oligothiophene Self-Assembly on the Surface of ZnO Nanorods: Toward Coaxial p-n Hybrid Heterojunctions. ChemPhysChem. 2009; 10:2465–2470. [PubMed: 19746390]
11. Olson DC, Lee YJ, White MS, Nikos K, Shaheen SE, Ginley DS, Voigt JA, Hsu JWP. Effect of Polymer Processing on the Performance of Poly(3-hexylthiophene)/ZnO Nanorod Photovoltaic Devices. J Phys Chem C. 2007; 111:16640–16645.
12. Ravirajan P, Peiro AM, Nazeeruddin MK, Graetzel M, Bradley DDC, Durrant JR, Nelson J. Hybrid Polymer/Zinc Oxide Photovoltaic Devices with Vertically Oriented ZnO Nanorods and an Amphiphilic Molecular Interface Layer. J Phys Chem B. 2006; 110:7635–7639. [PubMed: 16610853]
13. Coakley KM, Liu Y, McGehee MD, Frindell KL, Stucky GD. Infiltrating Semiconducting Polymers into Self-Assembled Mesoporous Titania Films for Photovoltaic Applications. Adv Funct Mater. 2003; 13:301–306.
14. Hung AM, Stupp SI. Simultaneous Self-Assembly, Orientaiton, and Patterning of Peptide-Amphiphile Nanofibers by Soft Lithography. Nano Letters. 2007; 7:1165–1171. [PubMed: 17447823]
15. Yang P, Deng T, Zhao D, Feng P, Pine D, Chmelka BF, Whitesides GM, Stucky GD. Hierarchically Ordered Oxides. Science. 1998; 282:2244–2246. [PubMed: 9856944]
16. Boeckler C, Feldhoff A, Oekermann T. Electrodeposited Zinc Oxide/Phthalocyanine Films- An Inorganic/Organic Hybrid System with Highly Variable Composition. Adv Funct Mater. 2007; 17:3864–3869.
17. Boeckler C, Oekermann T, Feldhoff A, Wark M. Role of the Critical Micelle Concentration in the Electrochemical Deposition of Nanostructured ZnO Films under Utilization of Amphiphilic Molecules. Langmuir. 2006; 22:9427–9430. [PubMed: 17042564]
18. Choi KS, Lichtenegger HC, Stucky GD, McFarland EW. Electrochemical Synthesis of Nanostructured ZnO Films Utilizing Self-Assembly of Surfactant Molecules at Solid-Liquid Interfaces. J Am Chem Soc. 2002; 128:12402–12403. [PubMed: 12381168]
19. Yoshida T, Minoura H. Electrochemical Self-Assembly of Dye-Modified Zinc Oxide Thin Films. Adv Mater. 2000; 12:1219–1222.
20. Spray RL, Choi K-S. Electrochemical Synthesis of SnO2 Films Containing Three-Dimensionally Organized Uniform Mesopores via Interfacial Surfactant Templating. Chem Commun. 2007:3655–3657.
21. Lee CW, Nam KW, Cho BW, Kim KB. Electrochemical Synthesis of Meso-Structured Lamellar Manganese Oxide Thin Film. Microporous and Mesoporous Materials. 2010; 130:208–214.
22. Yarger MS, Steinmiller EMP, Choi K-S. Electrochemical Synthesis of Cobalt Hydroxide Films with Tunable Interlayer Spacings. Chem Commun. 2007:159–161.
23. Tan Y, Srinivasan S, Choi KS. Electrochemical Deposition of Mesoporous Nickel Hydroxide Films from Dilute Surfactant Solutions. J Am Chem Soc. 2005; 127:3596–3604. [PubMed: 15755181]
24. Soci C, Zhang A, Xiang B, Dayeh SA, Aplin DPR, Park J, Bao XY, Lo YH, Wang D. ZnO Nanowire UV Photodetectors with High Internal Gain. Nano Letters. 2007; 7:1003–1009. [PubMed: 17358092]
25. Beek WJ, Wienk MM, Janssen RAJ. Hybrid Solar Cells from Regioregular Polythiophene and ZnO Nanoparticles. Adv Funct Mater. 2006; 16:1112–1116.
26. Law M, Greene LE, Johnson JC, Saykally R, Yang P. Nanowire Dye-Sensitized Solar Cells. Nature Materials. 2005; 4:455–459.

27. Quist PAC, Beek WJ, Wienk MM, Janssen RAJ, Savenije TJ, Siebbeles LDA. Photogeneration and Decay of Charge Carriers in Hybrid Bulk Heterojunctions of ZnO Nanoparticles and Conjugated Polymers. J Phys Chem B. 2006; 110:10315–10321. [PubMed: 16722734]

28. Steinmiller EMP, Choi KS. Anodic Construction of Lamellar Structured ZnO Films Using Basic Media via Interfacial Surfactant Templating. Langmuir. 2007; 23:12710–12715. [PubMed: 17973505]

29. Xing LL, Yuan B, Hu SX, Zhang YD, Lu Y, Mai ZH, Li M. Electrochemical Synthesis of Highly Oriented Layered Zinc Hydroxide with Intercalated *p*-Aminobenzoic Acid. J Phys Chem C. 2008; 112:3800–3804.

30. Bard, AJ.; Faulkner, LR. Electrochemical Methods: Fundamentals and Applications. 2. John Wiley & Sons, Inc; 2001.

31. Lee B, Park I, Yoon J, Park S, Kim J, Kim KW, Chang T, Ree M. Structural Analysis of Block Copolymer Thin Films with Grazing Incidence Small-Angle X-ray Scattering. Macromolecules. 2005; 38:4311–4323.

32. Renaud G, Lazzari R, Leroy F. Probing Surface and Interface Morphology with Grazing Incidence Small Angle X-Ray Scattering. Surface Science Reports. 2009; 64:255–380.

33. Renaud G, Lazzari R, Revenant C, Barbier A, Noblet M, Ulrich O, Leroy F, Jupille J, Borensztein Y, Henry CR, Deville JP, Scheurer F, Mane-Mane J, Fruchart O. Real-Time Monitoring of Growing Nanoparticles. Science. 2003; 300:1416–1419. [PubMed: 12775836]

34. Liu JF, Ducker WA. Surface-Induced Phase Behavior of Alkyltrimethylammonium Bromide Surfactants Adsorbed to Mica, Silica, and Graphite. J Phys Chem B. 1999; 103:8558–8567.

35. Arias AC, Granstrom M, Thomas DS, Petritsch K, Friend RH. Doped Conducting-Polymer--Semiconducting-Polymer Interfaces: Their Use in Organic Photovoltaic Devices. Phys Rev B. 1999; 60:1854–1860.

36. Kirchmeyer S, Reuter K. Scientific Importance, Properties and Growing Applications of Poly(3,4-ethylenedioxythiophene). J Mater Chem. 2005; 15:2077–2088.

37. Liang C, Shimizu Y, Masuda M, Sasaki T, Koshizaki N. Preparation of Layered Zinc Hydroxide/Surfactant Nanocomposite by Pulsed-Laser Ablation in Liquid Medium. Chem Mater. 2004; 16:963–965.

38. Ogata S, Miyazaki I, Tasaka Y, Tagaya H, Kadokawa J-i, Chiba K. Preparation Method for Organic-Inorganic Layered Compounds Including Fibrous Materials by the Reaction of Zn(OH)2 with Organic Compounds. J Mater Chem. 1998; 8:2813–2817.

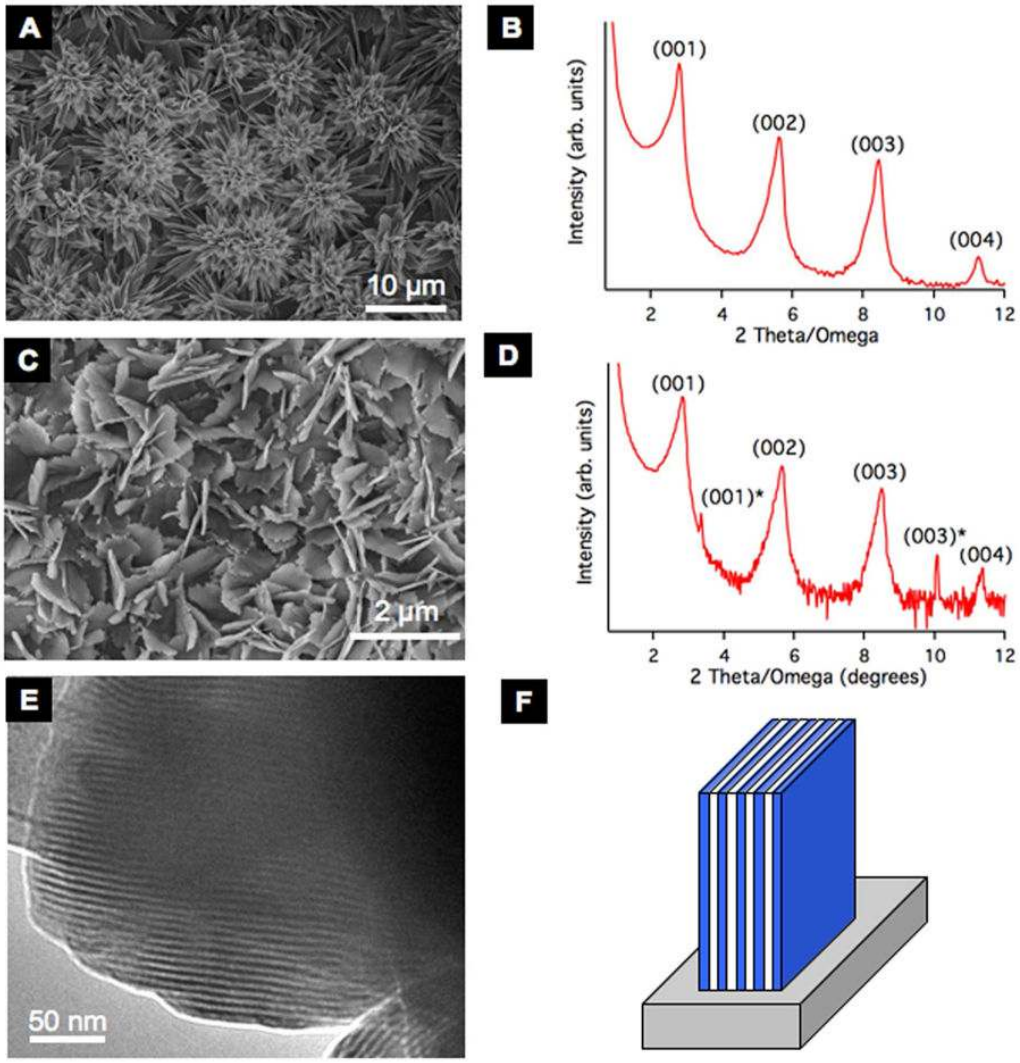

Figure 1.

(a), (c) SEM images showing the morphological differences for films electrodeposited for 20 mins in solutions of 50:50 (*v/v*) H_2O/DMSO, 0.04 M $Zn(NO_3)_2$ at two different surfactant concentrations: (a) 0.05 wt % PyBA and (c) 0.25 wt % PyBA. **(b), (d):** X-ray reflectivity measurements for (b) 0.05 wt % PyBA films, possessing a 3.2 nm lamellar periodicity and (d) 0.25 wt % PyBA films, possessing a 3.2 nm as well as 2.6 nm lamellar periodicity. **(e)** TEM image of the lamellar structure from the film grown in 0.05 wt % PyBA. The dark regions are the inorganic phase and the light regions are the organic domains. **(f)** Schematic represenation of the inorganic-organic lamellar structure growing perpendicular to the substrate surface.

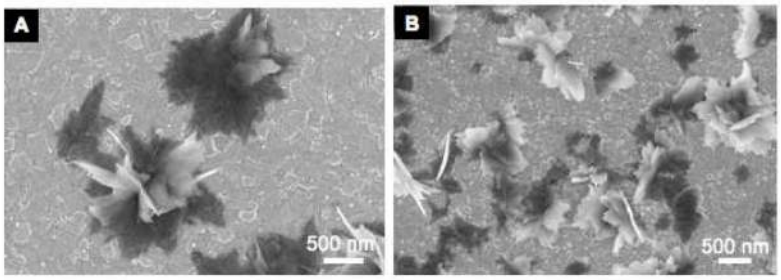

Figure 2.

UV-ozone treated ITO substrates electrodeposited for 1 min in solutions of 50:50 (*v/v*) H_2O/DMSO, 0.04 M $Zn(NO_3)_2$ at two different surfactant concentrations **(a)** 0.05 wt % and **(b)** 0.25 wt %.

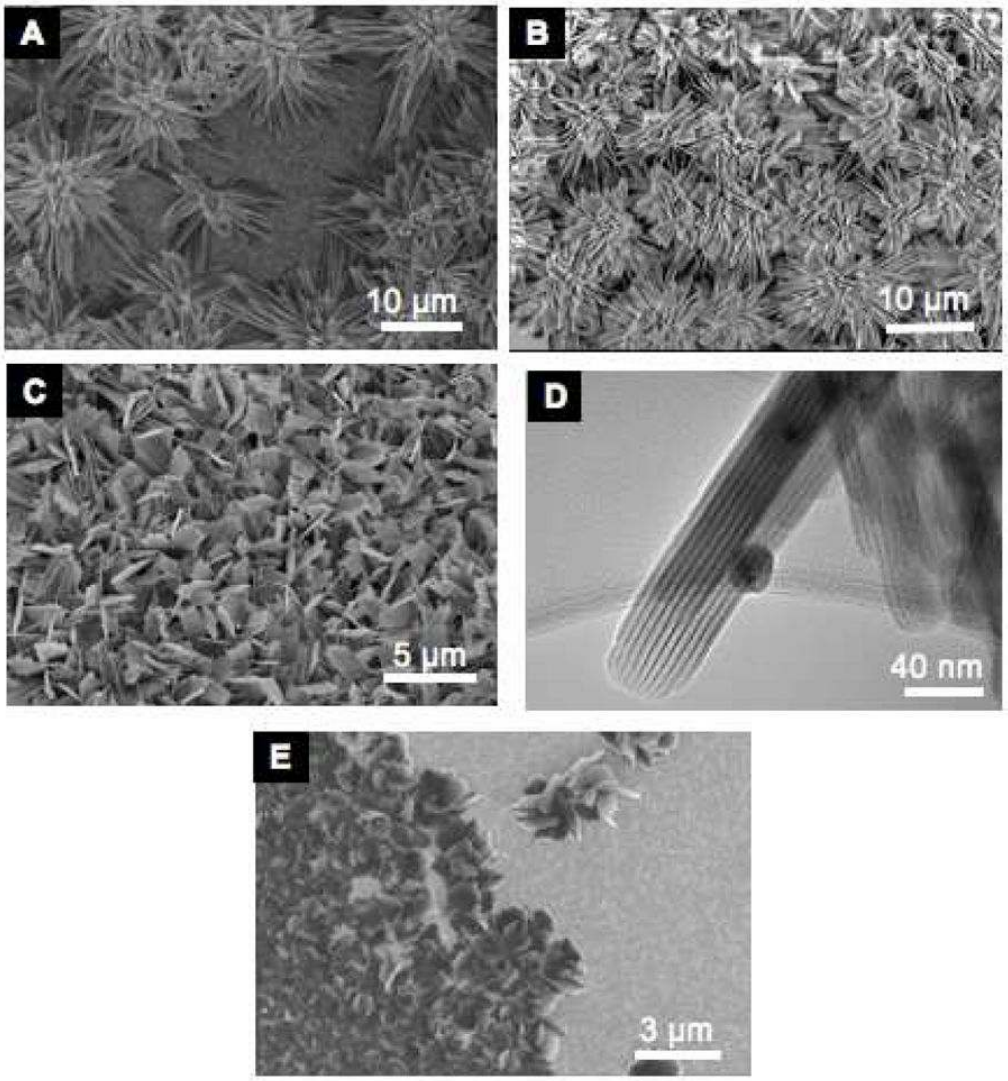

Figure 3.

(a)-(c) SEM images showing the change in morphology and alignment for films electrodeposited on UV-ozone treated ITO for 20 minutes in a solution of 0.05 wt % PyBA solution, 0.04 M $Zn(NO_3)_2$ and (a) 35:65 (*v/v*) H_2O/DMSO; (b) 50:50 (*v/v*) H_2O/DMSO; (c) 65:35 (*v/v*) H_2O/DMSO. **(d)** TEM image of the lamellar structure from the film grown in a solution with solvent composition 65:35 (*v/v*) H_2O/DMSO. **(e)** SEM image of a UV-ozone treated ITO substrate electrodeposited for 1 min in a solution with solvent ratio 65:35 (*v/v*) H_2O/DMSO.

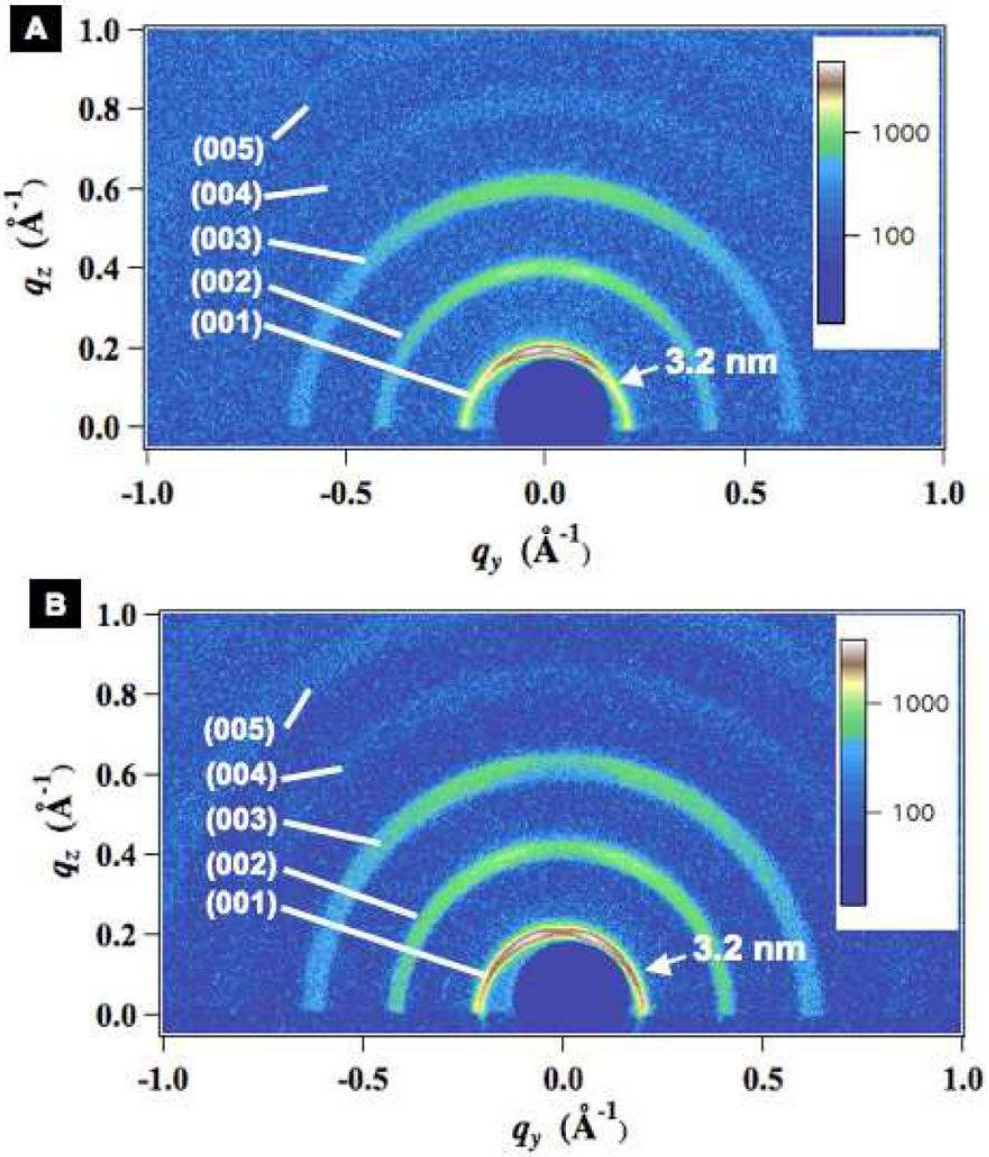

Figure 4.

2D-GISAXS data for films electrodeposited on UV-ozone treated ITO for 20 minutes in a solution of 0.05 wt.% PyBA solution, 0.04 M $Zn(NO_3)_2$ and **(a)** 50:50 (*v/v*) H_2O/DMSO (bloom-like growth); **(b)** 65:35 (*v/v*) H_2O/DMSO (flake-like growth). The nanoscale periodicity of both films is 3.2 nm.

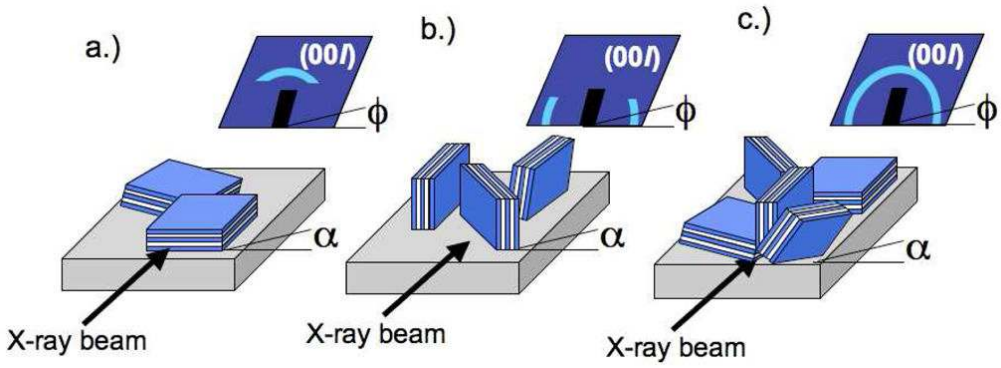

Figure 5.
Schematic diagram showing the relationship between lamellar orientation and the resulting 2D-GISAXS pattern: **(a)** lamellar structures oriented mostly parallel to the substrate surface; **(b)** lamellar structures oriented perpendicular to the substrate surface; **(c)** lamellar structures oriented randomly with respect to the substrate surface.

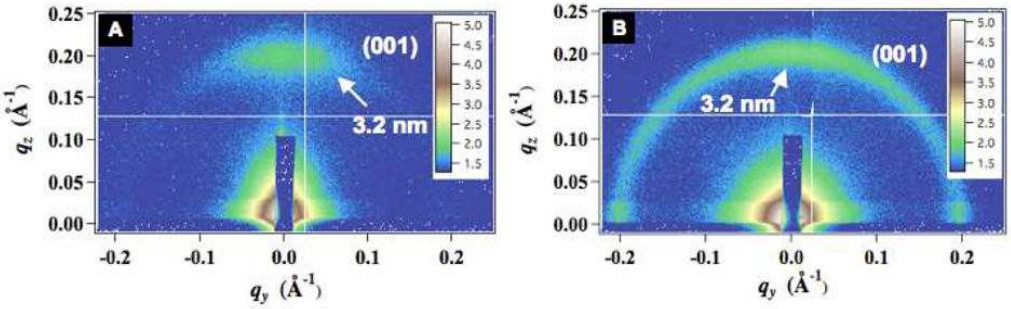

Figure 6.

2D-GISAXS data for films electrodeposited for short times on UV-ozone treated ITO in a solution of 0.05 wt.% PyBA solution, 0.04 M $Zn(NO_3)_2$ and 50:50 H_2O/DMSO, **(a)** after a deposition time of 30 s; **(b)** after a deposition time of 1 minute. The color scale is an arbitrary log scale.

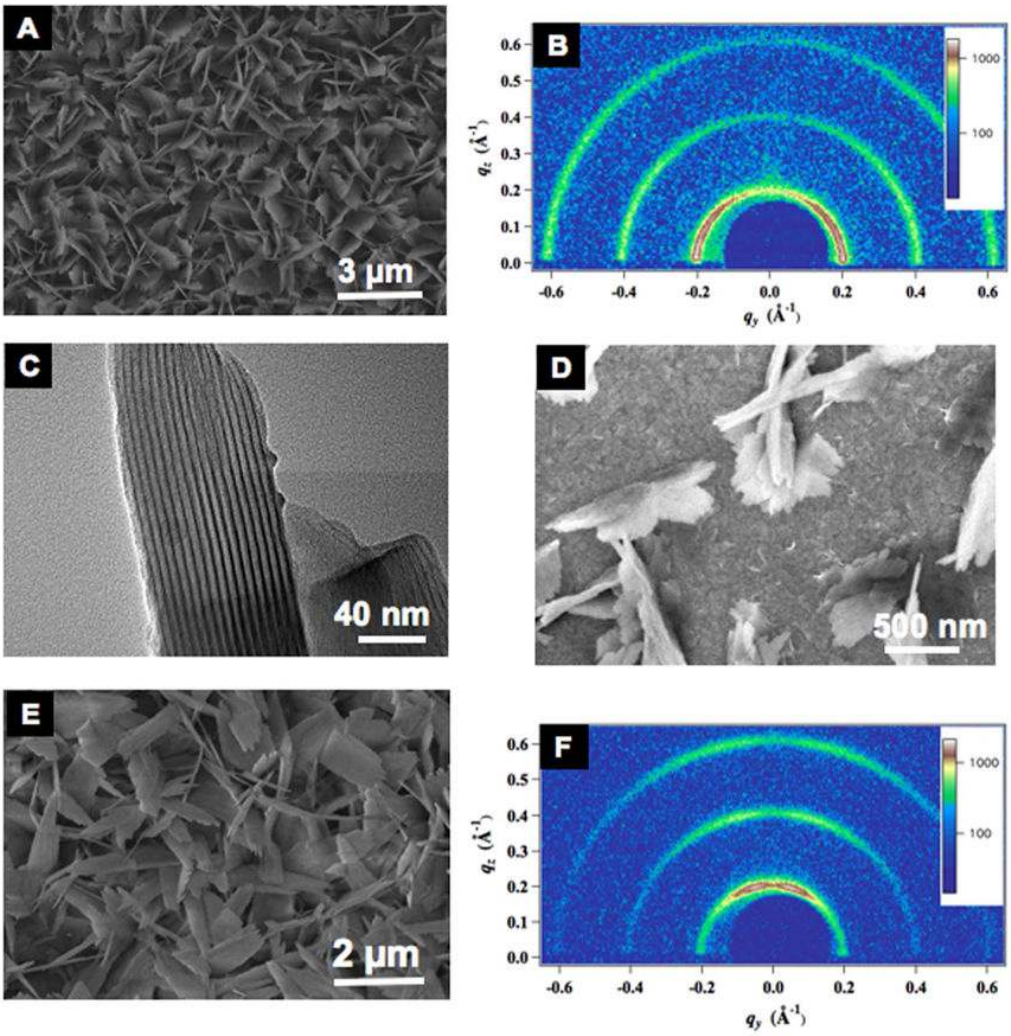

Figure 7.

(a) SEM image of the morphology of the lamellar structures grown on PEDOT:PSS coated ITO; **(b)** 2D-GISAXS image showing intensities corresponding to lamellar structures grown on PEDOT:PSS with strong perpendicular orientations; **(c)** TEM image showing the hybrid lamellar structure between the Zn-rich inorganic (dark regions) and the surfactant 1-pyrenebutyric acid (light regions); **(d)** Film electrodeposited for 1 minute in 50:50 (*v/v*) H_2O/DMSO, 0.05 wt.% PyBA, 0.04 M $Zn(NO_3)_2$ on PEDOT:PSS coated ITO; **(e)** SEM image of the morphology of the hybrid structures grown on PSS coated ITO; **(f)** 2D-GISAXS image showing intensities corresponding to lamellar structures grown on PSS with strong parallel orientations.